Copyright 2002 by the Society of Photo-Optical Instrumentation Engineers.

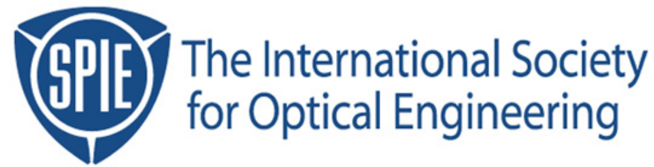

This paper was published in the proceedings of
Advances in Resist Technology and Processing XIX, SPIE Vol. 4690, pp. 952-962.
It is made available as an electronic reprint with permission of SPIE.

One print or electronic copy may be made for personal use only. Systematic or multiple reproduction, distribution to multiple locations via electronic or other means, duplication of any material in this paper for a fee or for commercial purposes, or modification of the content of the paper are prohibited.

Calibration of ESCAP Resist Simulation Parameters from Consideration of Printed CD Pitch Bias, CD Measurement Offset and Wafer Thermal History

Stewart A. Robertson[a], Doris Kang[a], Steven D. Tye[a],
Steven G. Hansen[b], Anita Fumar-Pici[b], Tsann-Bim Chiou[c],
Jeffery D. Byers[d], Chris A. Mack[d], and Mark D. Smith[d]

[a]Shipley Company Inc., 455 Forest Street, Marlborough, MA 01752
[b]ASML TDC, 8555 South River Parkway, Tempe, AZ 85284
[c]ASML TDC Taiwan, 10F-1, No. 6 Alley 99, Pu-Ding Road Hsinchu, Taiwan
[d]Parametric Solutions Division, KLA-Tencor Corporation,
8834 North Capital of Texas Highway, Suite 301, Austin, TX 78759

ABSTRACT

In this work an automated optimization routine is used to modify modeling parameters for a chemically amplified photoresist, with the goal of minimizing the error observed between lithography simulation and experimental results. It is shown that a basic tuning procedure modifying, optimizing only CD measurement offset and acid generation efficiency, improves the fit significantly. Further improvements can be made by optimization of the diffusion-deprotection kinetic parameters, in combination with the two aforementioned values. It is shown further improvement is observed if the actual temperature profile experienced in the postexposure bake process is considered and the temperature dependence of both the diffusion and the deprotection processes are optimized. This parameter values that result in this improvement infer a temporal offset in the start, and finish, of deprotection and acid diffusion.

Keywords: Lithography simulation, model calibration, hotplate, heat transfer, measurement offset

1. INTRODUCTION

The ongoing drive for faster and more densely packed integrated circuits requires ever decreasing geometries. Through the use of high numerical aperture lenses and migration to shorter exposing wavelengths, optical lithography continues to meet the industry requirements for resolution, dimension control and alignment, at acceptable cost. However, as feature dimensions reduce, optical proximity effects[1] become a significant issue. These effects mean that the printed resist feature dimensions are related not only to the size of the reticle feature but also to its proximity to adjacent structures. The most obvious example of this phenomenon is the relative print bias observed between lines of identical mask dimension set in different pitch ratios.[2]

The net outcome of these proximity effects is that when an advanced IC design is transferred to a reticle and exposed onto a wafer, the dimensional integrity between the realized pattern and the designed one is lost. Fortunately, this problem can be minimized through the application of Optical Proximity Correction (OPC)[3,4] a technique which uses assist features and fine biasing to overcome some of the dimensional errors caused by proximity effects.

Currently, OPC is applied in a rule-based manner with pitch. These rules are generated by laboriously examining a multitude of features (under a wide range of OPC conditions), then manually choosing the assist feature and fine bias configuration which minimizes the CD offset between pitches and maximizes the common process window.[5] To complicate these rules further, they are a strong function of illumination condition[6] and substrate reflectivity, so potentially a different set of rules is required for each critical process layer.

OPC rules could be generated rapidly, if lithographic simulation were used to assess optimum assist feature geometries and fine bias levels. Once initial work is done to generate appropriate resist models, the rules for various

substrates and stepper settings could be generated automatically. However, for this approach to be viable, it is necessary that the simulator is capable of accurately predicting the resist systems response to changes in nominal mask geometry, fine bias level and pitch.

It has been well documented that the diffusion length of PAC (photoactive compound) or photoacid affects cross-pitch bias.[7,8] Chemically amplified resists often exhibit non-Fickean diffusion (diffusivity changes during the PEB, either as a function of acid level or polymer deprotection). It has been shown that the parameters describing the variation in diffusivity also have a large impact on the predicted pitch bias[9].

Recent work[10], compared simulations utilizing an idealized PEB bake with those employing a realistic PEB temperature profile. The results showed that pitch bias was a function of the temperature rise and fall times.

In this work, the primary goal is to see whether model accuracy can be enhanced by considering the actual temperature profile experienced by the wafer and optimizing the deprotection and diffusion parameters for the photoresist.

2. EXPERIMENTAL WORK

2.1 Experimental CD Data

Wafers coated with UV™113 photoresist on AR2™ antireflectant were processed using an ASML PAS5500/300 stepper and a FSI Polaris 2100 series lithocluster, in accordance with the conditions described in Table 1. The proprietary dipole illumination scheme employed is described by Eurlings *et al.*[11]

A 21 column by 25 row Focus-Exposure Matrix (FEM) was shot, centered on a dose of 15.0 $mJcm^{-2}$ and a focal offset of 0.0 µm. The increments were 0.5 $mJcm^{-2}$ and 0.1 µm respectively.

The features of interest were nominal 130nm lines on the following pitch ratios; 1:1.0, 1:1.2, 1:1.4, 1:1.6 and 1:2.0. CD measurements were made for each feature at all points in the FEM.

Figure 1 shows the Bossung plot for the 1:1.6 pitch feature. Clearly, “best focus” occurs at a focus offset of +0.3 µm and the feature is correctly sized at a dose of 15.5 $mJcm^{-2}$. All cross pitch bias comparisons will be made at these conditions.

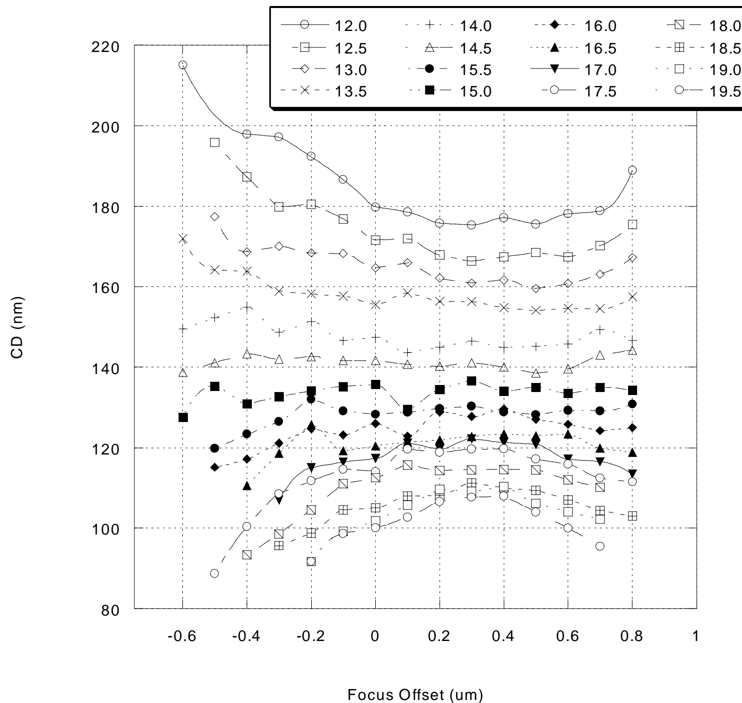

Figure 1: The experimental Bossung plot for the 130nm 1:1.6 lines

Substrate	200 mm Silicon
Antireflection Layer	60 nm AR2™ 60 Second Cure @ 205ºC
Resist	400 nm UV™113
Softbake	90 Seconds @ 130ºC
Exposure	ASML PASS5500/300 (KrF) 0.63 NA, Dipole Illumination 30º Pupil Blade, $0.8\sigma_{inner}/0.5\sigma_{outer}$
PEB	90 Seconds @ 130ºC
Development	60 Second Single Puddle 0.26N TMAH
CD Metrology	Hitachi S9200 CD SEM

Table 1: Experimental process conditions

2.2 Mask Dimensions

The binary test reticle used in this study was full characterized at the time of manufacture, using a KLA 8100 CD SEM. Table 2 details the mask dimension for each pitch of interest and gives the corresponding wafer scale dimension (4x smaller).

Pitch Ratio	Pitch Size	Mask Dimension	Wafer Scale Dimension
1:1.0	260 nm	536.4 nm	134.1 nm
1:1.2	286 nm	522.5 nm	130.6 nm
1:1.4	312 nm	538.0 nm	134.5 nm
1:1.6	338 nm	522.0 nm	130.5 nm
1:2.0	390 nm	529.8 nm	132.4 nm

Table 2: Measured reticle dimensions and corresponding wafer scale dimensions for nominal 130nm lines

2.3 Hotplate and Chillplate Characterization

A 9 point Sensarray Thermal Map2 *in-situ* process probe wafer was used to characterize a POLARIS PEB hotplate/chillplate combination. Figure 2 shows the resultant profile from one of the thermocouple positions. It is worth noting that it was necessary to manually transfer the probe wafer from the hotplate to the chill plate, so the handling time is significantly longer than in an automated mode.

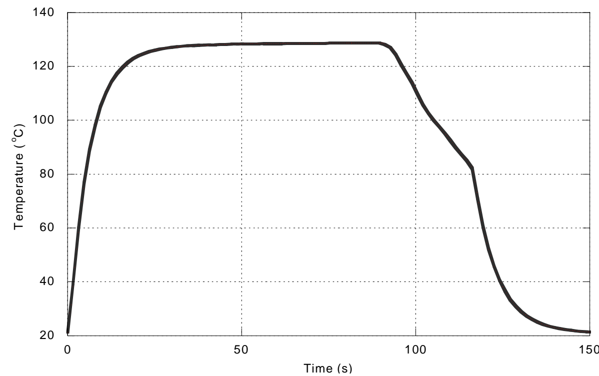

Figure 2: Measured temperature profile for POLARIS PEB hotplate/chillplate combination

In addition to the ideal bake scenario (where temperatures are assumed to change instantaneously to their setpoint values), PROLITH/2 V7.1 supports the use of an arbitrary time-temperature profile during the simulation of a PEB process. The profile may be entered in a tabular form or parametrically, using a simple three stage heat transfer model.

The three steps considered in the parametric model are heat transfer from the hotplate to wafer, ambient cooling during the transfer from hotplate to the chillplate and the forced cooling of the wafer on the chillplate. During each stage the temperature, T, at time, t, is given by[10]

$$T = (T_{initial} - T^*)\exp\left(-\frac{t}{\tau}\right) + T^* \tag{1}$$

where $T_{initial}$ is the wafer temperature at the beginning of the stage and T^* is the equilibrium temperature given by[10]

$$T^* = \frac{\frac{k_{air}}{\delta} T_{plate} + hT_{ambient}}{\frac{k_{air}}{\delta} + h} \tag{2}$$

where k_{air} is the thermal conductivity of air, δ is the thickness of the gap between the wafer and the hotplate or chillplate and h is a heat transfer coefficient for heat lost from the front of the wafer.

In equation (1), τ is the time constant for heating or cooling the wafer, given by[10]

$$\tau = \frac{\rho C_p L}{\frac{k_{air}}{\delta} + h} \tag{3}$$

where ρ is the density of silicon, C_p is the heat capacity of silicon and L is the thickness of the wafer.

Although the value of the equilibrium temperature, T^*, is not equal to the hotplate temperature, T_{plate}, it will typically be very close, since the proximity gap is very small, usually 150µm or less. Thus the solution to equation (1) can be simplified, with minimal error, by substitution T_{plate} for T^*.

A lumped value for τ can be determined without evaluating equation (3) by fitting equation (1) to an experimentally determined temperature profile.

Equation (1) fitted the observed bake profiles well and τ values were obtained for all three PEB stages, by averaging the behaviour observed at all nine wafer locations. The bake and handling times were adjusted to correspond to those actually observed during automated processing. Table 3 details the lumped capacitance model parameters required to model the POLARIS bake process. Interestingly, study of the experimental data revealed that the track started 2 seconds prior to starting its clock, resulting in an effective bake time longer than the dialed one.

Figure 3 compares the idealized bake with the actual bake cycle, as described by the three stage parametric lumped capacitance model.

Stage	Equilibrium Temperature, T^*	Time Constant, τ	Duration
Hotplate	130°C	6.6 sec	92.0 sec
Transfer	21°C	40.0 sec	7.0 sec
Chillplate	21°C	6.6 sec	30 sec

Table 3: Lumped capacitance model parameters for PEB process. The initial temperature for each stage is the final temperature of the previous stage

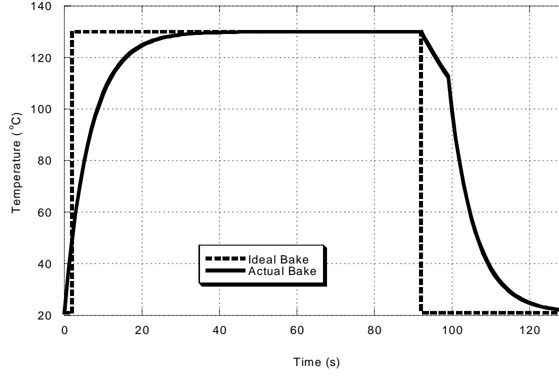

Figure 3: Comparison of ideal and actual PEB process temperature profiles

3. SIMULATION WORK

3.1 Simulation and Parameter Optimization Overview

All the simulations presented in this work utilized PROLITH2 v7.1 using the full scalar propagation model at a speedfactor of 6. The dipole illumination source was described using a database source file produced in MATLAB. Exact mask dimensions were employed and CD measurements were made using the weighted threshold measurement method with a 0.1% threshold, which is analogous to CD measurements at the substrate in a cross-sectional SEM image.

A previous study[7] indicated that simulated cross-bias pitch is relatively insensitive to speedfactor, CD measurement method and CD measurement threshold.

Parameter optimization is performed in an automatic manner using the AUTOTUNE option of Klarity ProDATA v1.3, as described Byers *et al.*[12] The optimization process relies on varying the input parameters to minimize the chi-squared (χ^2) function between the experimental and simulated data. The χ^2 function being a recognized measure of "goodness of fit" is defined as:

$$\chi^2(a) = \sum_{i=1}^{N}\left[\frac{y_i - y(x_i,a)}{\sigma_i}\right]^2 \tag{4}$$

where N = number of data points
(y_i,x_i) = the experimental data set
y = the predicted value
a = the simulated parameter set
σ = the uncertainty between y_i and the true data point

A related "goodness of fit" function is the root-mean-squared (RMS) error function, Σ.

$$\Sigma(a) = \sqrt{\frac{\chi^2(a)}{N}} = \sqrt{\frac{1}{N}\sum\left[\frac{y_i - y(x_i,a)}{\sigma_i}\right]^2} \tag{5}$$

Σ minimizes at the same input values as χ^2 but allows comparisons between datasets of differing size. The strategy employed for minimizing χ^2 is the two-step grid method described by Jug *et al.*[13]

Although the goal of this work is to optimize resist simulation parameters for the accurate prediction of cross-pitch print bias, ProDATA does not accept this data directly. Rather, CD information must be entered in FEM format, with a minimum matrix size of 3 by 3. This has the disadvantage of slowing down the optimization process by increasing the number of datapoints. However, the penalty is offset by the fact that there is greater confidence in the ability of the parameters to describe behavior in the focus and exposure planes.

In all the following calibrations, subsets of the full FEM data were used for each pitch. Each subset includes all FEM data spanning the dose range 15.0 – 17.5 $mJcm^{-2}$ and the focal range 0.0 to +0.50 μm.

3.2 Arrhenius Dependency

Many of the resist models within PROLITH assume that key parameters values, such as acid diffusivity and chemical amplification constant, can be defined as a function of bake temperature. In such cases, a simple Arrhenius dependence is assumed such that

$$P(T) = A_r \exp\left(\frac{-E_a}{RT}\right) \tag{6}$$

where $P(T)$ = a parameter which is a function of temperature
A_r = Arrhenius constant
E_a = activation energy
R = Universal gas constant
T = Temperature in Kelvin

It should be noted that for each temperature dependent value in PROLITH, the input values for the simulation are the activation energy and the natural logarithm of the Arrhenius constant.

3.3 Baseline Simulation Parameters

Baseline UV113 simulation parameters were determined from a basic manual tuning of experimentally measured optical, acid generation, deprotection, diffusion and dissolution rate information. The experimental methods and tuning procedures have been described at length elsewhere.[14-17] The baseline parameters assumed an ideal PEB temperature profile and were tuned to cross-sectional data for 180nm 1:1 line/space data from the manufacturer's literature.

In the baseline parameter set, the activation energies for both the PEB amplification and diffusion processes are set to zero (indicating no temperature dependence). The reason for this is twofold. Firstly, when considering an ideal bake situation, it is impossible to optimize both terms in the Arrhenius equation independently, since they are completely correlated. Secondly, chemically amplified resist simulation parameters are valid for only a single set of bake conditions and generally, cannot be extrapolated to other bake settings. Current softbake models apply only to undyed novolak materials, whilst diffusivity and deprotection models only consider Arrhenius changes in the PEB process, ignoring softbake effects. Previous work[15] has shown that parameters other than those described in terms of the Arrhenius equation must be altered to describe a resist's behaviour as the PEB temperature is changed.

3.4 Parameter Optimization

As with any set of uncalibrated parameters, it must be expected that a degree of basic tuning will be required to get quantitative agreement between experimental and simulated data. The baseline UV113 simulation parameters were generated on a different exposure system (at a different site) from the experimental dipole data and were tuned to cross-sectional data rather than top-down CD measurements.

Basic tuning practices proposed by Mack *et al.*[18] adjust acid generation efficiency C to compensate for exposure dose calibration differences, whilst work by Byers *et al.*[19] has shown that a CD offset between top-down CD SEM measurements and simulations (which more typically reflect cross-sectional measurements) is required to obtain optimum matches. To this end a CD measurement offset parameter has been added to the metrology setting in PROLITH/2 v7.1.

Based on these observations, an initial "basic tuning" was performed. This initial optimization retained the ideal PEB and the majority of the baseline parameters. Only the acid generation efficiency and the CD measurement offset were varied.

Having tried a basic tuning process, a more comprehensive optimization (still utilizing an idealized PEB bake) was undertaken. In addition to the two previously discussed values, the parameters controlling the PEB diffusion-

deprotection kinetic reaction were allowed to vary, i.e., the amplification reaction ln(A_r), the acid diffusivity ln(A_r) and the diffusivity ratio between blocked and unblocked polymer.

At this point the lumped parametric PEB hotplate model was introduced. Consequently, the use of both coefficients in the Arrhenius behavior models becomes appropriate since non-correlated optimization solutions are possible. Using the methods described elsewhere[20] activation energies for the chemical amplification factor and the diffusivity were determined for the photoacid/protecting group combination in UV™113. These values of 13.6 kcal.mol^{-1} and 71.7 kcal.mol^{-1}, respectively, were used for the seed values in the optimization process.

3.5 Optimization Results

Table 4 details the key baseline simulation parameters relating to the PEB kinetics, acid generation efficiency and the CD measurement offset. The Table also lists the final values of those parameters after each of the optimization processes. Accompanying each set of parameters are RMS error values for i) the FEM data used during the optimization and ii) the cross-pitch CD data at 15.5mJcm-2 (+0.3 µm focal offset).

Clearly, the baseline parameters do not correlate well with the experimental data. The basic tuning process significantly improves the results but requires a significant CD measurement offset and a large change in the acid generation efficiency. Figure 4 shows a plot of the experimental data, the baseline results (only one pitch fully resolved) and the tuned baseline results.

From the RMS error values it is clear that the fully optimized ideal bake scenario results in a considerable further enhancement of the fit. Whilst the revised acid generation efficiency remained similar, the improvements came from a reduction in the CD measurement offset and substantial changes to the diffusion and deprotection kinetics. Figure 5 compares simulated data with these parameters to the experimental results.

Introduction of the parametric bake and further optimization of the parameters results in a small, but measurable improvement in the fit. There are only small changes in the previously optimized acid generation efficiency, CD measurement offset and reacted/unreacted diffusivity ratio, and gratifyingly, the activation energy parameters optimize near their experimentally determined values. A comparison of experimental data and simulation for these values is also shown in Figure 5.

Parameter Name	Baseline Bake Parameters	Baseline Parameters with Basic Tune	Optimized Ideal Bake Parameters	Optimized Parametric Bake Parameters
Acid Generation Efficiency C	0.0441 cm^{2}mJ^{-1}	0.0794 cm^{2}mJ^{-1}	0.0766 cm^{2}mJ^{-1}	0.0792 cm^{2}mJ^{-1}
PEB Acid Diffusivity ln(Ar)	4.277 nm^{2}s^{-1}	4.277 nm^{2}s^{-1}	2.942 nm^{2}s^{-1}	92.926 nm^{2}s^{-1}
PEB Acid Diffusivity Ea	0.00 kcal.mol^{-1}	0.00 kcal.mol^{-1}	0.00 kcal.mol^{-1}	71.67 kcal.mol^{-1}
Initial Diffusivity @ 130°C	72.07 nm.s^{-2}	72.07 nm.s^{-2}	18.95 nm.s^{-2}	32.00 nm.s^{-2}
Diffusivity Variation	Linear	Linear	Linear	Linear
Reacted/Unreacted Diffusivity Ratio	0.08	0.08	0.4984	0.4975
PEB Amplification Reaction ln(Ar)	-0.3470 s^{-1}	-0.3470 s^{-1}	-0.3660 s^{-1}	16.983 s^{-1}
PEB Amplification Reaction Ea	0.00 kcal.mol^{-1}	0.00 kcal.mol^{-1}	0.00 kcal.mol^{-1}	13.986 kcal.mol^{-1}
PEB Amplification Factor @ 130°C	0.707	0.707	0.694	0.617
Room Temp. Acid Diffusion Length	0.00 nm	0.00 nm	0.00 nm	0.00 nm
Amplification Reaction Order	1.34	1.34	1.34	1.34
Relative Quencher Concentration	0.264	0.264	0.264	0.264
PEB Diffusion-controlled Reaction	27400	27400	27400	27400
PEB Bulk Acid Loss	None	None	None	None
PEB Acid Evaporation	None	None	None	None
CD Measurement Offset	0.0 nm	26.80 nm	15.62 nm	17.47 nm
Group FEM RMS Error (Σ)	162.64 nm	11.59 nm	3.60 nm	3.51 nm
Cross Pitch RMS Error (Σ)	131.69 nm	4.92 nm	2.81 nm	2.35 nm

Table 4: Key simulation parameters for the UV™113 photoresist process, prior to and after the various optimization strategies

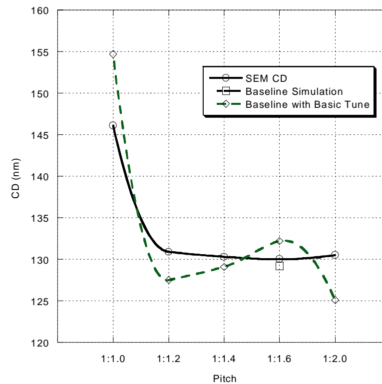

Figure 4: Experimental CD data comparison to simulations using (a) the baseline parameter set and (b) the "tuned" baseline parameter set (exposure = 15.5 mJcm^{-2}, focal offset = +0.3µm)

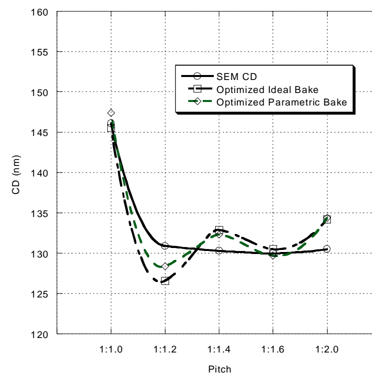

Figure 5: Experimental CD data comparison to simulations using (a) the fully optimized ideal bake parameter set and (b) the fully optimized parametric bake parameter set (exposure = 15.5 mJcm^{-2}, focal offset = +0.3µm)

4. DISCUSSION OF RESULTS

4.1 Verification of CD Measurement Offset

During the various optimization procedures CD measurement offset values of between 15 and 27 nm were predicted. In an attempt to gauge the accuracy of these values, which were determined solely by "goodness of fit", an experimental estimate of the offset was made by measuring the "actual" resist feature CD by cross-section SEM and comparing the values to the CD SEM data. Cross-sectional data was gathered for each pitch at our nominal dose and focus. Table 5 compares the CD measurements from the two methods. Although there is some spread in the observed offset the average value is 16.6 nm, which is very close to the final values obtained in both the full ideal bake optimization and the full parametric bake optimization.

4.2 Cross-pitch CD Response

Inspection of Figures 4 and 5 indicates that the simulated CD data appears to oscillate with pitch ratio whilst the experimental results appear to vary in a smooth monotonic manner. When the entire set of CD data within the various focus-exposure matrices is considered, it appears that the experimental data at the particular conditions studied in these two figures is atypical and other conditions seem to exhibit the oscillatory pattern seen in the simulations. For example, Figure 6 shows the experimental and fully optimized simulation fits for an adjacent point in the FEM array (exposure = 15.0 mJcm^{-2}, focal offset = +0.3µm). At this focus and exposure setting it is apparent that both experimental

and simulated data are exhibiting the same oscillatory behavior. As the mask dimensional data predicts a slight oscillatory trend and the RMS error is good for the fit to each FEM, it can be concluded that the lack of oscillations in the case studied, in particular is probably due to noise in the experiment. In order to avoid this phenomenon in future, it would be more appropriate to fit an analytical function to the data and optimize the parameters to match that fit or utilize CD data from several replicates of the same experiment.

Pitch Ratio	Pitch Size	Top-Down SEM CD	X-Section SEM CD	Delta CD
1:1.0	260 nm	146.1 nm	128 nm	18.1 nm
1:1.2	286 nm	130.9 nm	110 nm	20.9 nm
1:1.4	312 nm	130.3 nm	113 nm	17.3 nm
1:1.6	338 nm	130.0 nm	118 nm	12.0 nm
1:2.0	390 nm	130.5 nm	115 nm	14.5 nm
Mean Top-Down to X-Section SEM CD Delta				16.6 nm

Table 5: Comparison of top-down CD SEM measurements and cross-section SEM CD measurements

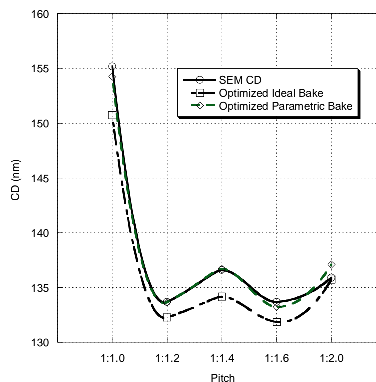

Figure 6: Experimental CD data comparison to simulations using (a) the fully optimized ideal bake parameter set and (b) the fully optimized parametric bake parameter set (exposure = 15.0 $mJcm^{-2}$, focal offset = +0.3µm)

4.2 Diffusion-Deprotection Kinetics during PEB

The use of the parametric bake over the ideal bake resulted in an improved fit to the experimental data. Inspection of the diffusivity and chemical amplification factors during the PEB process may give insight to the reason why. Figure 7 shows a plot of these values as a function of time for the fully optimized fit. The values were calculated by substituting the wafer temperature into the Arrhenius equation (6). In the ideal bake scenario both diffusion and deprotection would start simultaneously, however in the situation shown in Figure 7, it is apparent that significant chemical amplification occurs before any diffusion. Effectively, a delay has been inserted between the onset of deprotection and the onset of diffusion.

Whilst the values presented result in enhanced modeling capabilities, this does not necessarily mean that this is what occurs in the resist, since the model is a gross simplification of reality. In actuality, acid diffuses in one direction, base quencher diffuses in the other, solvent loss and glass transition temperature changes modify diffusivity and so on.

5. CONCLUSIONS

It has been demonstrated that the lumped capacitance parametric bake model in PROLITH v7.1 fits experimental data from an actual PEB process very well.

If this heat transfer model is employed over the normal ideal model, it is possible to find resist simulation parameters which match experimental results more closely. However, it should be noted that the improvement in results is fairly marginal and comes at the expense of additional optimization time since an additional two parameters need to be fitted.

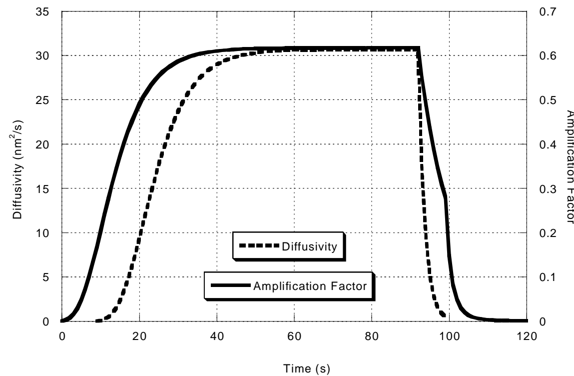

Figure 7: Diffusivity and chemical amplification factor values during the simulated PEB process

6. ACKNOWLEDGEMENTS

The authors would like to thank Mike Reilly of Shipley Company for providing the dipole illuminator file.

7. REFERENCES

1. B.J. Lin, "Methods to print optical images at low-k_1 factors", *Optical/Laser Microlithography III*, SPIE Vol. 1264, pp. 2-12, 1990.
2. C.A. Mack, "Optical proximity effects, Part 3", *Microlithography World*, Vol. 5, No. 4, pp. 23 – 24, Autumn 1996.
3. J.F. Chen, T. Laidig, K.E. Wampler and R. Caldwell, "Full-chip optical proximity correction with depth of focus enhancement", *Microlithography World*, Vol. 6, No. 3, pp. 5 –13, Summer 1997.
4. J.F. Chen, T. Laidig, K.E. Wampler, R. Caldwell, K.H. Nakagawa and A. Liebchen, "A practical technology path to sub-0.10 micron process generations via enhanced optical lithography", *19th Annual Symposium on Photomask Technology*, SPIE Vol. 3873, pp. 995 – 1016, 1999.
5. M.T. Reilly, C.R. Parker, K. Kvam, R.J. Socha and M.V. Dusa, "Comparison of OPC rules and common process windows for 130-nm features using binary and attenuated phase-shift masks", *Optical Microlithography XIII*, SPIE Vol. 4000, pp. 1209 – 1222, 2000.
6. M.T. Reilly, C.R. Parker, F. Fischer and T. Hiar, "Maximizing common process latitude by integrated process development for 130 nm lithography", *Optical Microlithography XV*, SPIE Vol, 4691, Paper 77, 2002.
7. S. A. Robertson, E. K. Pavelchek, C. I. Swible-Keane, J. F. Bohland and M. T. Reilly, "Factors affecting pitch bias in lithography simulation", *Optical Microlithography XIII*, SPIE Vol. 4000, pp. 744 –758, 2000.
8. B. Tolkuehn, M. Hoepfl, A. Erdmann, S. Majoni and M. Jess, "Automatic resist parameter calibration procedure for lithographic simulation", *Lithography for Semiconductor Manufacturing II*, SPIE Vol. 4404, pp. 313 – 324, 2001.

9. A. Erdmann, W. Henke, S.A. Robertson, E. Richter, B. Tolkuehn and W. Hoppe, "Comparison of simulation approaches for chemically amplified resists", *Lithography for Semiconductor Manufacturing II*, SPIE Vol. 4404, pp. 99 – 110, 2001.
10. M. D. Smith, C. A. Mack and J. S. Petersen, "Modeling the impact of thermal history during post exposure bake on the lithographic performance of chemically amplified resists", *Advances in Resist Technology and Processing XVIII*, SPIE Vol. 4345, pp 1013 – 1021, 2001.
11. M. Eurlings, E. van Settien, J.A. Torres, M.V. Dusa, R.J.Socha, L. Capodieci and J. Finders, "0.11 μm imaging in KrF lithography using dipole illumination", *Lithography for Semiconductor Manufacturing II*, SPIE Vol. 4404, pp. 266 – 278, 2001.
12. J.D. Byers, C.A. Mack, R. Huang and S. Jug, "Automatic calibration of lithography simulation parameters using multiple data sets", *MNE 2001*, Paper PH7, 2001.
13. S. Jug, R. Huang, J. D. Byers and C. A. Mack, "Automatic calibration of lithographic simulation parameters", *Lithography for Semiconductor Manufacturing II*, SPIE Vol. 4404, pp. 380 – 395, 2001.
14. S.A. Robertson, C.A. Mack and M. Maslow, "Towards a universal resist dissolution model for lithography simulation", *Lithography for Semiconductor Manufacturing II*, SPIE Vol. 4404, pp. 111 - 122, 2001.
15. D. Kang, E.K. Pavelchek and C.I. Swible-Keane, "The accuracy of current model descriptions of a DUV photoresist", *Advances in Resist Technology and Processing XVI*, SPIE Vol. 3678, pp 877 - 890, 1999.
16. T.H. Fedynyshyn, J.W. Thackeray, J.H. Georger and M.D. Denison, "Effect of acid diffusion on performance in positive deep ultraviolet resists", *J. Vac. Sci. Tecnhol. B*, Vol. 12, pp. 3888 – 3894, 1994.
17. C.R. Szmanda, R.J. Kavanagh, J.R. Bohland, J.F. Cameron, P. Trefonas and R.F. Blacksmith, "Simple method for measuring acid generation quantum efficiency at 193 nm", *Advances in Resist Technology and Processing XVI*, SPIE Vol. 3678, pp. 857 – 866, 1999.
18. C.A. Mack, M. Ercken and M. Moelants, "Matching simulation and experiment for chemically amplified resists", *Optical Microlithography XII*, SPIE Vol. 3679, pp. 183 – 192, 1999.
19. J.D. Byers, W.B. Howard, M. Pochkowski and C.A. Mack, "Determining and improving the predictability of lithography simulation", *Advances in Resist Technology and Processing XIX*, SPIE Vol. 4690, Paper 43, 2002.
20. D. Kang and S.A. Robertson, "Measuring and simulating postexposure bake temperature effects in chemically amplified photoresists", *Advances in Resist Technology and Processing XIX*, SPIE Vol. 4690, Paper 112, 2002.